CHEMISTRY OF MATERIALS
Cite This: Chem. Mater. 2019, 31, 2002−2009
Article
pubs.acs.org/cm

Stabilizing Sulfur Cathode in Carbonate and Ether Electrolytes: Excluding Long-Chain Lithium Polysulfide Formation and Switching Lithiation/Delithiation Route

Xiaona Li,[†,∥,⊥] Jianwen Liang,[†,⊥] Weihan Li,[†,‡] Jing Luo,[†] Xia Li,[†] Xiaofei Yang,[†] Yongfeng Hu,[§] Qunfeng Xiao,[§] Wanqun Zhang,[∥] Ruying Li,[†] Tsun-Kong Sham,[‡] and Xueliang Sun*[,†]

[†]Department of Mechanical and Materials Engineering and [‡]Department of Chemistry, University of Western Ontario, London, Ontario N6A 5B9, Canada

[§]Canadian Light Source, Saskatoon, Saskatchewan S7N 2V3, Canada

[∥]Hefei National Laboratory for Physical Science at Microscale, Department of Chemistry, University of Science and Technology of China, Hefei, Anhui 230026, P. R. China

Supporting Information

ABSTRACT: Due to the inevitable chemical reactions between the nucleophilic lithium polysulfides and electrophilic carbonate solvents, conventional S cathodes are incompatible in carbonate-based electrolytes. Alternative ether-based electrolytes are confronted with another concern of the dissolution of long-chain Li_2S_x ($4 \le x \le 8$) intermediates. Herein, originally designed strategy to stabilize S cathodes in these two electrolytes was proposed by introducing central Fe linkers to switch the lithiation/delithiation route from the formation of long-chain Li_2S_x intermediates to Li_yFeS_x intermediates. Based on this, amorphous FeS_x/C (a-FeS_x/C, x = 2, 4, 6) composites, synthesized by comelting ferrocene and sulfur, were demonstrated as effective cathodes for Li−S batteries. a-FeS_4/C cathode delivers a remarkably high capacity of 931 mAh g^{-1} at 0.1 A g^{-1} and a stable cycling performance of over 500 cycles in a carbonate electrolyte without any compatibility problem. Good cyclability with high capacity is also demonstrated in a $LiNO_3$-free ether electrolyte.

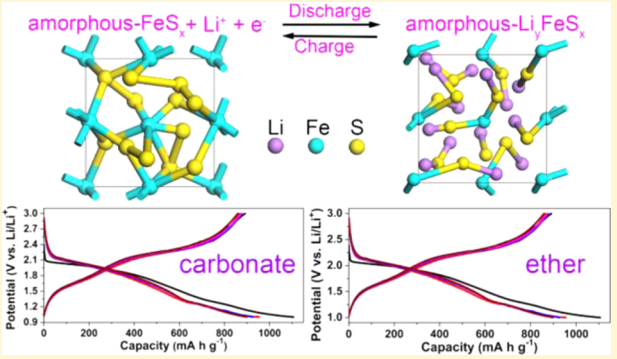

INTRODUCTION

Lithium−sulfur (Li−S) batteries are a promising next-generation system with high theoretical specific capacity (1675 mAh g^{-1}) and energy density (2600 Wh kg^{-1}).[1] However, sulfur cathodes still face many challenges, especially the chemical unstability of lithium polysulfide intermediates (Li_2S_x, x = 4−8) in liquid electrolytes. In ether-based electrolytes, the long-chain polysulfides can be dissolved in the electrolyte and chemically reduced on the lithium anode surface.[2−4] Such reactions would lead to both passivations of the lithium anode by forming an insulating surface layer (mainly composed of Li_2S_2 and Li_2S) and generation of low-order polysulfides that shuttle back to the cathode to be recharged to higher-order polysulfides, resulting in the so-called shuttling effects in Li−S batteries. In carbonate-based electrolytes, the inevitable chemical reactions between the nucleophilic Li_2S_x intermediates and electrophilic solvents can trigger continuous decomposition. The widely used carbonate-based electrolytes in lithium-ion batteries are generally incompatible in Li−S batteries.[5−7]

Although sulfur cathodes with various host materials are able to show reduced polysulfide dissolutions and deliver feasible performance in the ether-based electrolyte, Li−S batteries bare no tolerance of any polysulfide dissolution in the carbonate-based electrolyte due to their irreversible chemical reaction. To date, only a few sulfur-based composite cathodes have been proved successful in carbonate-based electrolytes, such as pyrolyzed polyacrylonitrile sulfur composites,[8,9] sulfur molecules confined in microporous carbon composites,[10] Se_xS_y/C composites,[11,12] and molecular layer-deposited alucone-coated S/C electrodes.[13] The common feature of those cathodes is the tailored sulfur cathode structure to alter the reaction route to solid-state electrochemical conversion; thus, severe side reactions could be avoided to a great extent in carbonate-based electrolytes.

More recently, emerging amorphous transition metal polysulfide cathodes (NbS_x,[14] MoS_x,[15,16] and TiS_x[17]) have also been proved feasible and show unique electrochemical property in the carbonate-based electrolytes. For example, amorphous niobium polysulfides (a-NbS_x (x = 3−5)) exhibited reversible

Received: November 30, 2018
Revised: February 25, 2019
Published: February 27, 2019

DOI: 10.1021/acs.chemmater.8b04987
Chem. Mater. 2019, 31, 2002−2009

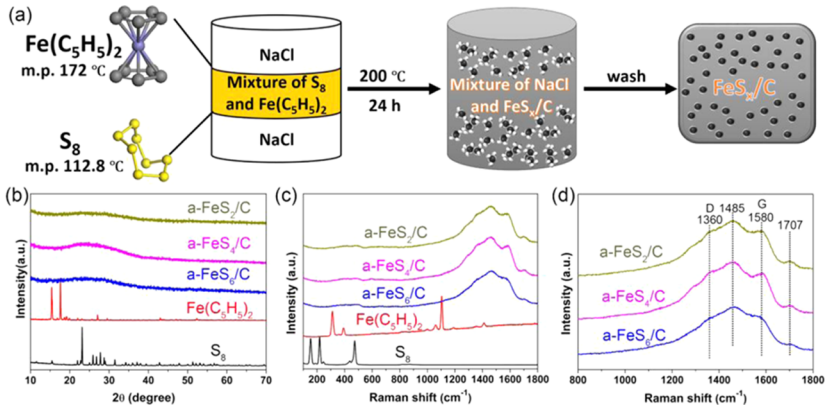

Figure 1. Synthetic route of a-FeS_x materials and characterization. (a) Schematic illustration of the preparation of a-FeS_x/C composites. (b) X-ray diffraction (XRD) patterns of commercial S_8, $Fe(C_5H_5)_2$, and the as-prepared a-FeS_x/C samples. (c, d) Raman spectra of commercial S_8, $Fe(C_5H_5)_2$, and the as-prepared a-FeS_x/C samples.

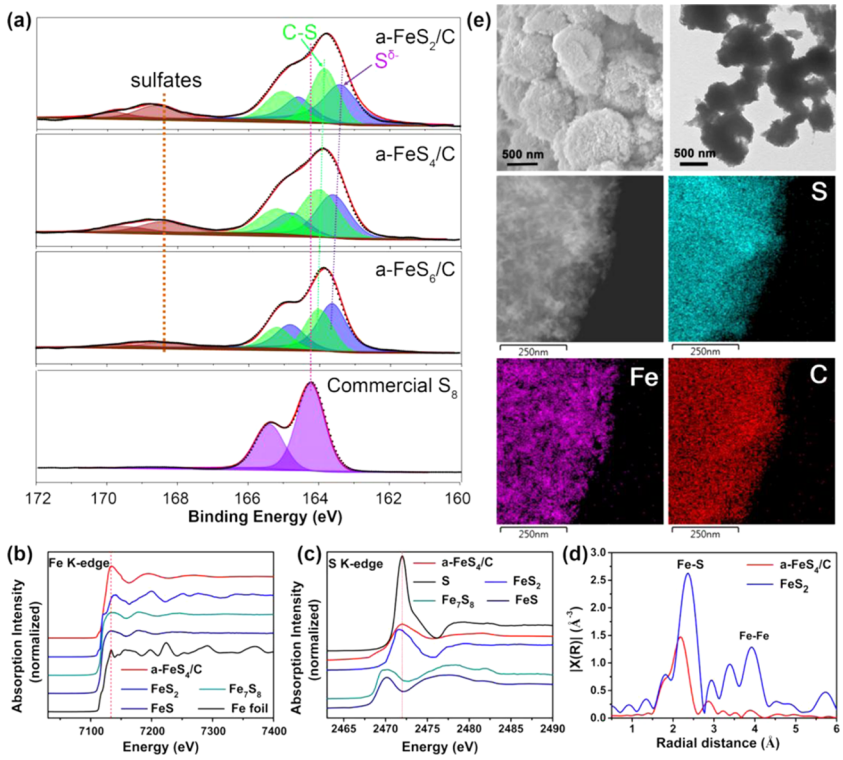

Figure 2. Structure analysis of a-FeS_x/C composites. (a) S 2p XPS spectra of the a-FeS_x/C composites and commercial S_8. (b) Normalized Fe K-edge X-ray absorption spectra (XAS) of a-FeS_4/C in comparison with commercial FeS_2, Fe_7S_8, FeS, and metallic Fe. (c) Normalized S K-edge ex situ X-ray absorption near-edge structure (XANES) spectra of a-FeS_4/C sample in comparison with commercial FeS_2, FeS, Fe_7S_8, and S_8. (d) Fourier transform of the Fe K-edge extended X-ray absorption fine structure (EXAFS) spectra (R space) of a-FeS_4/C and commercial FeS_2. (e) Scanning electron microscopy (SEM) and transmission electron microscopy (TEM) images of the a-FeS_4/C composite, and the scanning transmission electron microscopy (STEM) image of the a-FeS_4/C sample and corresponding energy-dispersive X-ray spectroscopy (EDX) elemental maps.

lithiation/delithiation process in a carbonate-based electrolyte, with an average discharge voltage of about 2 V and an initial discharge capacity of up to 596 mAh g^{-1}.[14] The authors pointed out that amorphization was an effective approach to increase the capacities of niobium polysulfides. Amorphous molybdenum polysulfide chalcogels ($MoS_{3.4}$), prepared through the oxidation of $(NH_4)_2MoS_4$ by iodine, were also reported with good performance in a carbonate-based electrolyte, delivering an initial discharge capacity of approximately 600 mAh g^{-1}.[15] It is demonstrated that those amorphous transition metal polysulfides exhibit sulfur-like electrochemical behaviors and transition metal function as "linkers" to prevent the formation of unstable long-chain polysulfide.

Herein, for the first time, the switched lithiation/delithiation route for sulfur cathodes in liquid electrolytes by introducing central Fe linkers to exclude long-chain lithium polysulfide formation is presented. The proposed amorphous FeS_x/C (a-FeS_x/C, x = 2, 4, 6) cathodes could not only operate effectively in a $LiNO_3$-free ether-based electrolyte but also operate in a common carbonate-based electrolyte. Synchrotron-based X-ray absorption near-edge spectroscopy coupled with other characterization techniques proved that (1) no free S_8 molecule exists in the a-FeS_x/C composites and (2) the anchoring effects

DOI: 10.1021/acs.chemmater.8b04987
Chem. Mater. 2019, 31, 2002−2009

provided by the central Fe atoms during the lithiation/delithiation process guarantee the formation of Li_yFeS_x intermediates rather than unstable long-chain Li_2S_x intermediates. This study clearly showed that a structure-oriented electrochemical reaction mechanism/route for the sulfur cathode expands the possibilities of sulfur-based cathodes in carbonate electrolytes.

RESULTS AND DISCUSSION

To synthesize the amorphous FeS_x/C (a-FeS_x/C) composites, ferrocene ($Fe(C_5H_5)_2$), with a melting point of 172−174 °C, was mixed with commercial sulfur followed by heating at 200 °C for 24 h in a confined space sealed by NaCl (Figure 1a). During the heating process, $Fe(C_5H_5)_2$ reacted with sulfur to form amorphous FeS_x within the molten system. Here, x denotes the molar ratio of Fe to S (x = 2, 4, 6) and corresponds to the reaction stoichiometry. Meanwhile, amorphous carbon was obtained from the chemical decomposition of $Fe(C_5H_5)_2$ in the confined spaces. Corresponding compositions of the a-FeS_x/C samples were characterized by elemental analysis and inductively coupled plasma atomic emission spectroscopy analysis, as shown in Table S1, which showed a similar molar ratio of Fe to S as the raw materials. The carbon content in the a-FeS_x/C composites was about ∼28−33 wt %, decreasing with increasing x.

X-ray diffraction (XRD) analysis (Figures 1b and S1) confirms the amorphous/disordered structure, and there are four Raman peaks for the a-FeS_x/C composites (Figure 1c,d), which is quite different from that of traditional crystalline FeS_2[18] (XRD pattern in Figure S2, Raman spectra in Figure S3). The Raman peak at 1360 cm^{-1} is attributed to D mode vibration of graphite crystallites at the edges, and the peak at 1580 cm^{-1} corresponded to G mode of carbon, which involved the stretching motion of sp^2-bonded carbon atoms in a two-dimensional hexagonal lattice.[19] The shift of G mode (∼20 cm^{-1}) suggested a specific structure of carbon through the formation of the C−S_m chains, which is similar to the reported carbyne polysulfide.[20] This shift was related to the synthesis approach, where the carbon was derived from ferrocene consisting of two cyclopentadienyl rings.[20,21] The peak at 1485 cm^{-1} possibly resulted from the partial hydrogenation of the amorphous carbon,[22] which is consistent with the elemental analysis results. The origin of the peak at 1707 cm^{-1} is unclear, but the four Raman peaks are presumably characteristic peaks of the unique amorphous carbon formed from the reaction at a relatively low temperature. Briefly, the absence of $Fe(C_5H_5)_2$ or S characteristic peaks confirmed the complete reaction between $Fe(C_5H_5)_2$ and sulfur. The different vibrational information compared with FeS_2 also indicates the different chemical bonds and symmetry between a-FeS_x/C composites and FeS_2. Differential scanning calorimetry (DSC, Figure S4) analysis further confirms the amorphous structure. Different from the obvious endothermic peaks of commercial S_8 and crystalline FeS_2 (Figure S4a,b), no endothermic peaks were observed for the a-FeS_2/C and a-FeS_4/C samples (Figure S4c,d), suggesting good thermal stability, and there is no free sulfur in the samples, whereas for the a-FeS_6/C sample, there is a small endothermic peak at 200 °C, demonstrating the phase transformation at that temperature.

X-ray photoelectron spectroscopy (XPS) was employed to analyze the chemical state of elements for the a-FeS_x/C composites. As shown in Figure 2a, the S 2p spectra of a-FeS_x/C were composed of three sets of doublet peaks (S $2p_{3/2}$ and S $2p_{1/2}$), with S $2p_{3/2}$ peaks located at 163.4, 163.8, and 168.5 eV, respectively. The presence of the S $2p_{3/2}$ peak at 168.5 eV indicated the formation of sulfur−oxygen bond (surface sulfate, SO_4^{2-}) due to partial surface oxidation of the samples (Figure S5).[23] As for the other two S $2p_{3/2}$ peaks, although there is a slight energy shift among the a-FeS_x/C samples, the binding energies were substantially lower than 164.0 eV of the elemental S_8. This demonstrated the different electronic state of sulfur in the a-FeS_x/C samples compared to that of elemental S_8. Furthermore, the high-energy shift of the a-FeS_4/C and a-FeS_6/C samples compared to that of the a-FeS_2/C sample should be originated from the less degree of electron bond polarization of sulfur along with the higher sulfur content in the sample. Although the S $2p_{3/2}$ peak at 163.4 eV has been reported as bridge sulfur in a long chain linked by central inorganic atoms in amorphous transition metal polysulfides,[23,24] S $2p_{3/2}$ peaks located at 163.4−163.8 eV were attributed to the C−S bond in sulfur-based composites in other studies.[21,25] Since the binding energies of these two interactions were too close to be differentiated, the two S $2p_{3/2}$ peaks at 163.4 and 163.8 eV are generally assigned to sulfur interaction with iron or carbon in the a-FeS_x/C samples.

Typical synchrotron radiation-based X-ray absorption spectroscopy (XAS) of a-FeS_4/C sample was conducted under protection, as shown in Figure 2b−d. The absorption peak of Fe K-edge arose from the transition of Fe 1s core electrons to the unoccupied 4p states. The absorption peak of Fe K-edge of a-FeS_4/C shifted to a lower energy than that of FeS_2 and was different from any other typical Fe−S compounds (FeS_2, Fe_7S_8, FeS, and Fe). Moreover, the long-range X-ray absorption region of the a-FeS_4/C sample exhibited a relatively flat curve, which was consistent with its amorphous structure. The local structures (R space) of Fe atom for the FeS_2 and a-FeS_4/C samples were characterized by Fourier transform (FT) of extended X-ray absorption fine structure (EXAFS) (the amplitude of the FT of the EXAFS ($\chi(k)k^2$)) and are compared in Figure 2d. The R space of the commercial FeS_2 showed characteristic peaks at approximately 1.86 and 3.40 Å (it is not phase-corrected; so, the bond length is smaller than the real crystalline value, Figure S6).[26] The peaks observed at 1.86 Å was attributable to the Fe−S bond (2.269 Å, Figure S6), whereas the peak observed at 3.40 Å was mainly related to the Fe−Fe bond (3.838 Å, Figure S6). These results are consistent with the previous reports.[27] The a-FeS_4/C sample contained Fe−S referred to the peak of 1.67 Å, whereas the features were quite different from that in the crystalline FeS_2. Moreover, the peak intensity for the Fe−Fe bonds in the R space was significantly diminished in the a-FeS_4/C spectrum. This is expected since the EXAFS shows no long-range order. Consequently, the local structures of Fe were different between a-FeS_4/C and FeS_2. Unlike the crystalline FeS_2, some polysulfide bonds had been formed around the central Fe atoms in the a-FeS_4/C, with longer and irregular interatomic distance leading to the dispersion of the Fe atoms. At the same time, the S K-edge (Figure 2c) absorption of a-FeS_4/C exhibited a white line peak in between those of FeS_2 and S, suggesting that the chemical state of the S element in a-FeS_4/C sample was between those in FeS_2 and S with large unoccupied densities of states of p character. The low oxidation states of S should result from stronger Fe−S interaction locally. Scanning electron microscopy (SEM) and transmission electron microscopy (TEM) images in Figure 2e show that the a-FeS_4/C product is predominantly composed of nanosized flocky spheres. The scanning transmission electron

DOI: 10.1021/acs.chemmater.8b04987
Chem. Mater. 2019, 31, 2002−2009

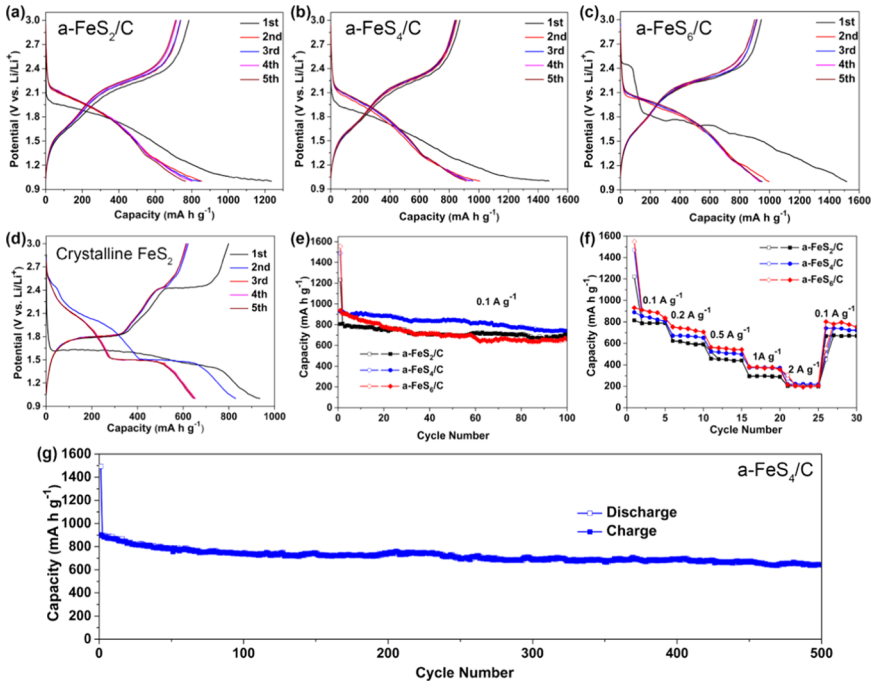

Figure 3. Electrochemical performance in carbonate electrolytes (1 M $LiPF_6$ in EC/DEC (1:1, v/v)). (a–d) Charge/discharge curves of the a-FeS_x/C and crystalline FeS_2 electrodes in 1.0–3.0 V versus Li/Li^+ at 0.1 A g^{-1}. (e) Cycling performance of the a-FeS_x/C electrodes at 0.1 A g^{-1}. (f) Rate capabilities of the a-FeS_x/C electrodes at the current densities from 0.1 to 2 A g^{-1}. (g) Long-term cycling performance of the a-FeS_4/C electrode at 0.1 A g^{-1} for 500 cycles.

microscopy (STEM) image and corresponding energy-dispersive X-ray spectroscopy (EDX) elemental maps for the a-FeS_4/C sample (Figure 2e) confirm the even distribution of S, Fe, and carbon within the sample.

Figure 3 shows the electrochemical performance of the a-FeS_x/C electrodes in a carbonate-based electrolyte of 1 M $LiPF_6$ in ethylene carbonate/diethyl carbonate (EC/DEC) (1:1, v/v). Figure 3a–c depicts the discharge/charge curves of the a-FeS_x/C cells at 0.1 A g^{-1} for the first five cycles. All three a-FeS_x/C electrodes presented analogous discharge/charge curves of similar shape and voltage but possessed increasing capacities with increasing sulfur content. The a-FeS_2/C, a-FeS_4/C, and a-FeS_6/C electrodes delivered an initial discharge capacity of 1236, 1474, and 1526 mAh g^{-1}, respectively. However, as indicated by the obvious discharge plateau at around 2.45 V (Figure 3c), part of the initial discharge capacity of the a-FeS_6/C electrode was actually contributed from the irreversible side reactions between long-chain polysulfides and the carbonate electrolyte. The irreversibility problem is also common for traditional sulfur cathodes in carbonate electrolyte,[13] but the problem appeared to be resolved using the a-FeS_2/C or a-FeS_4/C electrode, as indicated by the absence of the extra discharge plateau. The resulting charge capacities of a-FeS_2/C, a-FeS_4/C, and a-FeS_6/C electrodes were 803, 931, and 944 mAh g^{-1}, respectively.

The subsequent discharge/charge curves were stabilized and became very similar for the three a-FeS_x/C electrodes, with an average discharge plateau at about 1.8 V and a small shoulder at roughly 1.3 V, arising from the stepwise reduction of the polysulfide cathode.[28] The charge curves exhibited a minor plateau at ∼1.65 V and a major plateau at ∼2.25 V. The galvanostatic intermittent titration technique analysis provided equilibrium discharge/charge curves of the same shape but with smaller polarizations (Figure S7). In contrast, the crystalline FeS_2 presented a distinctive two-step discharge curve (Figure 3d) with more than half of the capacity delivered below 1.5 V. The stabilized discharge capacity of the crystalline FeS_2 electrode (∼650 mAh g^{-1}) was also substantially smaller than that of the a-FeS_2/C electrode (∼800 mAh g^{-1}) with a similar chemical formula. The relatively sloping and smooth discharge/charge profiles of the a-FeS_x/C electrode indicated continuous Li^+ storage sites within the a-FeS_x/C electrodes.[29,30]

Figure 3e compares the cycling stability of the three a-FeS_x/C electrodes at 0.1 A g^{-1}. Except for the initial few cycles, the a-FeS_4/C electrode maintained the highest capacities over 100 cycles. The discharge capacities of the a-FeS_2/C, a-FeS_4/C, and a-FeS_6/C electrodes were 696, 735, and 671 mAh g^{-1}, respectively, at the 100th cycle. It is not surprising that the a-FeS_6/C electrode faded more quickly than the other two because of the occurring side reactions with the carbonate electrolyte discussed earlier, as well as the possible structural change caused by the multielectron electrochemical reactions.[14] Even after 500 cycles, the a-FeS_4/C electrode still maintained a high discharge capacity of 644 mAh g^{-1} (Figure 3g). Additionally, all of the a-FeS_x/C electrodes exhibited acceptable rate performance, as shown in Figure 3f. Consistent with previous discussions, a higher sulfur content of the a-FeS_x/C electrode leads to a higher capacity overall. This trend was more obvious at low current rates and vanished at high current rates. When returning to the low current rate of 0.1 A g^{-1} after the high-rate cycling, the a-FeS_x/C electrodes almost recovered the capacities before high-rate testing, indicating that the high-rate performance was limited by kinetics rather than structural deformation. Nevertheless, the reversible capacities or the capacity retentions of the three a-FeS_x/C electrodes have well exceeded most reported metal polysulfide materials[14−17] and crystalline FeS_2 cathodes (Tables S2 and S3). The homogeneous distribution of iron, sulfur, and carbon in the a-FeS_x/C

DOI: 10.1021/acs.chemmater.8b04987
Chem. Mater. 2019, 31, 2002−2009

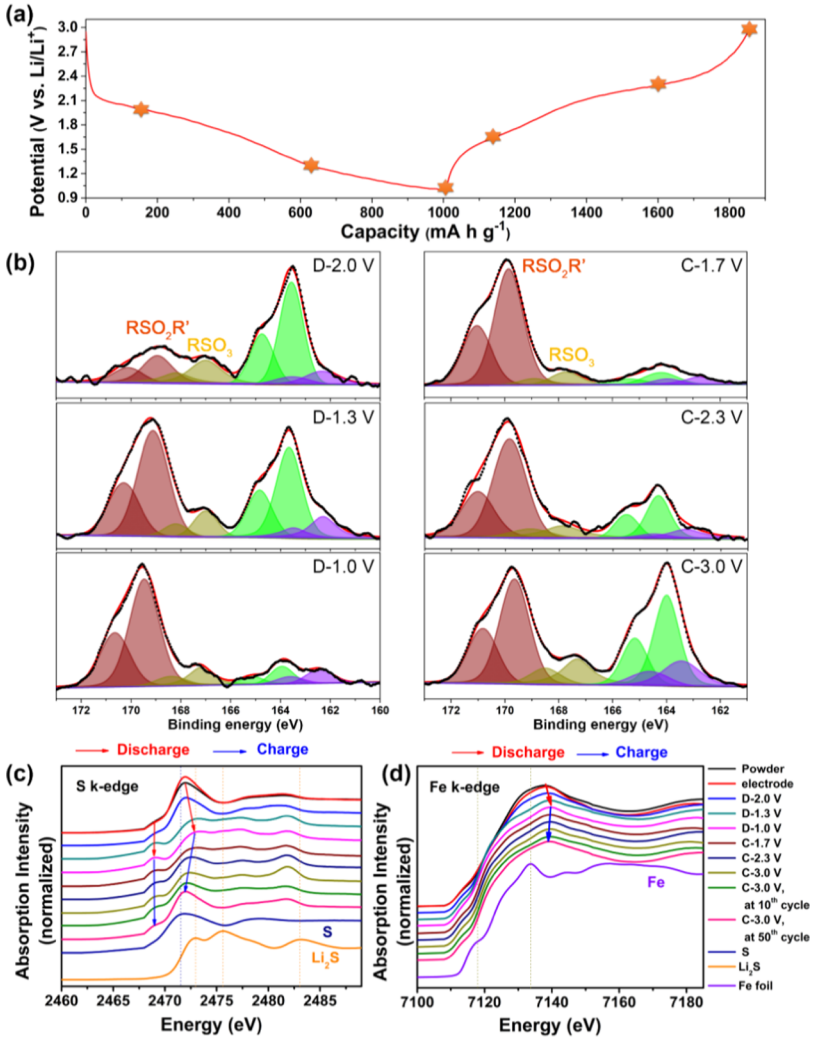

Figure 4. Postmortem characterization of the a-FeS_4/C electrode in carbonate electrolyte. (a) Typical discharge/charge curve of the a-FeS_4/C electrode at 0.1 A g^{-1}. (b) Ex situ XPS spectra of S 2p for a-FeS_4/C cathodes at different discharged or recharged states. The cells were discharged to 2.0, 1.3, and 1.0 V or recharged to 1.7, 2.3, and 3.0 V. (c, d) Evolution of S K-edge and Fe K-edge XANES spectra of a-FeS_4/C electrode during the first lithiation/delithiation process and the full delithiation state after cycles.

electrodes should be helpful to ensure the effective confinement of sulfur. EDX maps of the a-FeS_4/C electrode after 100 cycles still showed even distributions of the three constituents with no obvious agglomeration of sulfur (Figure S8).

To investigate the electrochemical reaction mechanism, the a-FeS_4/C cathode discharged and charged to various states in carbonate electrolyte was analyzed by XPS (Figure 4a). During the discharge process (Figure 4b), the emerging S $2p_{3/2}$ peaks at 169.2 and 167.1 eV indicated the formation of sulfur oxidation groups ($RSO6_2R'$ and RSO_3, respectively)[31] as the solid electrolyte interface (SEI) components on the surface of the a-FeS_4/C cathode. The increasing peak intensities of the sulfur oxidation groups with deeper state of discharge suggested the thickening of SEI during discharge. Basically, the results are consistent with previous reports about other types of sulfur cathodes in the carbonate-based electrolyte, indicating that the formation of SEI layer on the surface of cathodes is also important for the quasi-solid electrochemical reaction.[12,13,31] In addition, the other sulfur peaks could be split into other two S $2p_{3/2}$ peaks at 163.7 and 162.3 eV. The former peak showed decreasing intensity upon discharging, whereas the latter peak behaved oppositely, indicating the reduction of sulfur as the active material in the composite. Since the S 2p level of S^{2-} state is known to span the energy range of 160−162.7 eV,[32,33] the S $2p_{3/2}$ peak at 162.3 eV was most reasonably attributed to the reduced sulfur components in the discharged state. However, no signal was observed at around 160.5 eV for Li_2S[32] even when the electrode was discharged to 1.0 V (Figure 4b). The remaining S $2p_{3/2}$ peak at 163.7 eV also suggested an incomplete reduction of sulfur. The S $2p_{3/2}$ peak at a higher binding energy (green peaks in Figure 4b) increased upon charging, suggesting that most of the reduced sulfur were reoxidized upon delithiation of the cathode. The XPS spectra evolution of the iron component during discharge/charge was also studied (Figure S9). Basically, the Fe 2p XPS spectra of the a-FeS_4/C cathode at all discharged or charged states are very similar apart from the weak signal obtained at full discharge, which might be influenced by the SEI formation on the cathode surface. Moreover, these Fe 2p XPS spectra are different from that of the initial state of a-FeS_4/C cathode before cycling (Figure S5b), indicating the variation of the chemical state compared to that before electrochemical reaction, and no signal due to $Fe^{(0)}$ is observed.

Ex situ X-ray absorption near-edge structure (XANES) spectra of Fe K-edge and S K-edge for the a-FeS_4/C cathode

DOI: 10.1021/acs.chemmater.8b04987
Chem. Mater. 2019, 31, 2002−2009

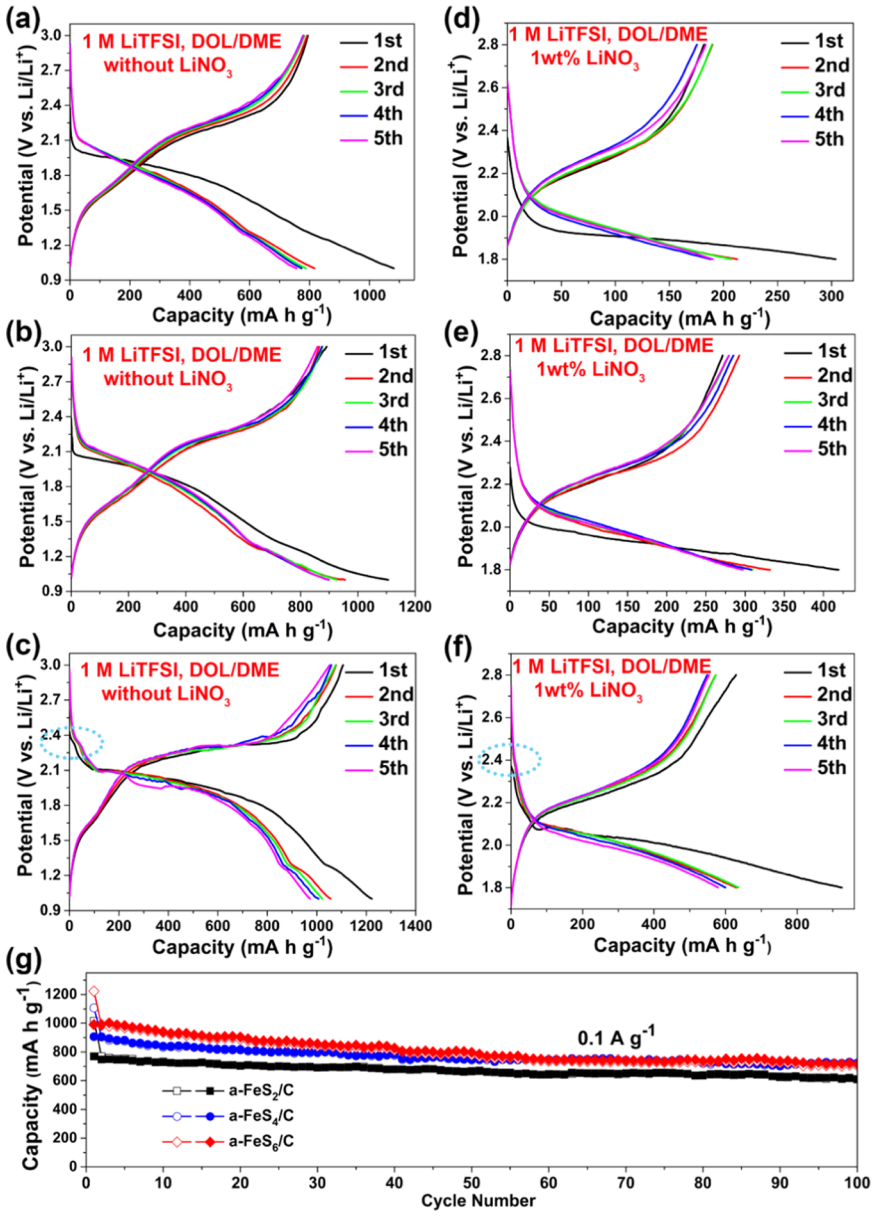

Figure 5. Electrochemical performance of the a-FeS_x/C electrodes in ether electrolyte. (a−c) Charge/discharge curves of the a-FeS_x/C electrodes in the potential region of 3.0−1.0 V versus Li/Li^+ at 0.1 A g^{-1}. The electrolyte here was 1 M LiTFSI in DOL/DME (1:1, v/v) free of $LiNO_3$. (d−f) Charge/discharge curves of the a-FeS_x/C electrodes in the potential region of 2.8−1.8 V versus Li/Li^+ at 0.1 A g^{-1}. The electrolyte here was 1 M LiTFSI in DOL/DME (1:1, v/v) with 1 wt % $LiNO_3$. (g) Cycling performance of the a-FeS_x/C electrodes in the potential region of 3.0−1.0 V versus Li/Li^+ at 0.1 A g^{-1}. The electrolyte here was 1 M LiTFSI in DOL/DME (1:1, v/v) free of $LiNO_3$.

were also measured under protection at different states (Figure 4c,d). Throughout the discharge/charge cycle, the white line peaks of the S K-edge XANES spectra for the a-FeS_4/C cathode were located between those of Li_2S and S_8 (Figure 4c). The peak gradually shifted toward higher energy during discharging and recovered to the original position upon recharging, and highly reversible redox reactions of S were observed. Notably, characteristic peaks of Li_2S_x (at ~2468 and 2469.5 eV[13,16]) were absent from the discharge/charge process, demonstrating that the electrochemical process of a-FeS_4/C was free of soluble Li_2S_x intermediates and thus stable against carbonate electrolyte. Fe K-edge XANES spectra evidenced that the iron component was also reduced during discharge and oxidized during charge (Figure 4d), whereas no metallic Fe generated among the whole lithiation/delithiation process. After 10 or 50 cycles, the spectra of a-FeS_4/C at fully charged state remained highly similar to that measured for the first cycle. Good reversibility of a-FeS_4/C cathode was inferred.

Based on the XPS and XANES results, the electrochemical reaction of the a-FeS_4/C cathode did not involve the formation of any metallic Fe and Li_2S_x intermediates. Reasonable reaction route combines both intercalation/deintercalation and conversion reaction simultaneously, as similar to the reported amorphous TiS_4 cathodes.[17] During the lithiation process, the coordination number of Fe decreased with the increasing Li content, whereas the Fe component still maintained the −Fe−S− chains in the amorphous Li_yFeS_x intermediates.[29] Thus, central Fe atoms within the a-FeS_x/C composites would anchor S atoms during cycling, with the formation of solid Li_yFeS_x intermediates rather than soluble Li_2S_x species.

DOI: 10.1021/acs.chemmater.8b04987
Chem. Mater. 2019, 31, 2002−2009

The electrochemical properties of the a-FeS_x/C electrodes were further generalized in the ether-based electrolytes with or without the $LiNO_3$ additive. Because of the serious polysulfide dissolution problems and the resulting shuttling effects for common sulfur cathodes, $LiNO_3$ is often used as a consuming additive to passivate the lithium anode surface and control the polysulfide shuttling effects. However, the side reactions between $LiNO_3$ and cathodes below ~1.8 V have limited its feasible electrochemical window and thus have to sacrifice the undervoltage capacities. Herein, taking the advantage of the a-FeS_x/C cathodes to abstain from polysulfide intermediates, cells using a $LiNO_3$-free electrolyte of 1 M LiTFSI in dioxolane/dimethoxyethane (DOL/DME; 1:1, v/v) were tested. The corresponding discharge/charge curves at 0.1 A g^{-1} between 1.0 and 3.0 V are shown in Figure 5a−c. The performance of the a-FeS_x/C electrodes was very similar to that in the carbonate-based electrolyte (Figure 3a−c), except for the polysulfide (Li_2S_x, $4 < x < 8$) plateau at around 2.35 V in the a-FeS_6/C cell rather than a side-reaction plateau at about 2.45 V (Figure 5c versus Figure 3c). When the electrolyte was added with 1 wt % $LiNO_3$, the operating voltage window was adjusted to 1.8−2.8 V to avoid unfavorable reactions of $LiNO_3$. As demonstrated in Figure 5d−f, the a-FeS_x/C electrodes exhibited typical discharge/charge curves that were exactly corresponding to the portion in the same voltage range of the $LiNO_3$-free cells. The $LiNO_3$ additive obviously helped to reduce shuttling effects (particularly, the suppression of overcharge) in the a-FeS_6/C cell but at a cost of significant capacity reduction due to the restricted voltage range. On the other hand, the $LiNO_3$ additive was completely unnecessary for the a-FeS_2/C and a-FeS_4/C cells because their electrochemical mechanisms were free of polysulfide intermediates in the first place.

The cycling stabilities of the a-FeS_x/C electrodes in the $LiNO_3$-free ether-based electrolyte are shown in Figure 5g. Similar to the performance in the carbonate-based electrolyte, the higher the sulfur content of the a-FeS_x/C electrode, the higher is the initial reversible capacity. The first-cycle discharge/charge capacities of the a-FeS_2/C, a-FeS_4/C, and a-FeS_6/C electrodes were 1016/770, 1107/906, and 1223/990 mAh g^{-1}, respectively. Although the a-FeS_6/C electrode had the highest initial reversible capacities, the stable a-FeS_4/C electrode readily showed the comparable capacity to the faded a-FeS_6/C electrode after about 50 cycles. After 100 cycles, the discharge capacities of the a-FeS_2/C, a-FeS_4/C, and a-FeS_6/C electrodes were 610, 721, and 704 mAh g^{-1}, respectively. In addition, the coulombic efficiency of the two stable electrodes, a-FeS_2/C and a-FeS_4/C, was close to 100%, whereas the lower coulombic efficiency (referring to a larger charge capacity than discharge capacity) of the a-FeS_6/C electrode indicated the presence of polysulfide shuttling effects (Figure S10).

After disassembling the cycled cells (Figure S11), the obvious dissolution of lithium polysulfides in the a-FeS_6/C cell was confirmed by the apparent yellow color on the separator and lithium metal anode, as well as the serious corrosion of the lithium metal anode. In contrast, neither the obvious coloration of the separator nor lithium metal corrosion was observed in the a-FeS_2/C and a-FeS_4/C cells. The ultraviolet−visible spectra of the three a-FeS_x/C electrodes after 30 cycles also proved similar results (Figure S12). The a-FeS_6/C electrode showed a significantly high intensity of polysulfide (S_n^{2-}, $4 \le n \le 6$) peaks,[34] whereas the corresponding peaks were relatively weak for the other two electrodes.

CONCLUSIONS

In summary, we demonstrate a highly efficient approach to achieve excellent cyclability of sulfur cathode in both carbonate and $LiNO_3$-free ether-based electrolytes by simply introducing central Fe linkers to exclude long-chain lithium polysulfide formation. The proposed novel amorphous FeS_x/C (a-FeS_x/C, x = 2, 4, 6) composites could be obtained by a facile synthesis approach of comelting reaction between ferrocene and excess sulfur at 200 °C. Multiple characterization methods (including XRD, DSC, XPS, and XANES) demonstrated that there is almost no free sulfur in the a-FeS_x/C composites, especially the a-FeS_2/C and a-FeS_4/C composites. Evidently, the a-FeS_x/C electrodes undergo a unique electrochemical reaction mechanism, involving continuous lithiation/delithiation pathways with varying lithium content in the form of the Li_yFeS_x intermediates rather than the unstable long-chain lithium polysulfides.

ASSOCIATED CONTENT

Supporting Information

The Supporting Information is available free of charge on the ACS Publications website at DOI: 10.1021/acs.chemmater.8b04987.

Additional experimental methods, XRD patterns, Raman spectra, differential scanning calorimetry tests, crystal structure, galvanostatic intermittent titration technique, STEM and corresponding EDX elemental maps, XPS spectra, coulombic efficiency, digital photographs of the disassembled cells, UV−visible absorption spectra, and comparison with recent works on metal polysulfides and crystalline FeS_2 cathodes in lithium ion batteries (PDF)

AUTHOR INFORMATION

Corresponding Author

*E-mail: xsun9@uwo.ca.

ORCID

Xueliang Sun: 0000-0003-2881-8237

Author Contributions

⊥X.L. and J.L. contributed equally to this work.

Author Contributions

X.L. and J.L. contributed equally to this work. X.L. and J.L. conceived the project, designed the electrochemical and characterization experiments, which X.L. then performed. W.L., Y.H., Q.X., and T.-K.S. analyzed and interpreted the XAS experimental data. X.L. and X.Y. performed the SEM and XPS experiments and analyzed the data. W.Z. performed the XRD and STEM experiments and analyzed the data. X.L. drafted the paper with support from J.L. All authors discussed the results and commented on the manuscript. The work was supervised by X.S.

Notes

The authors declare no competing financial interest.

ACKNOWLEDGMENTS

This research was supported by the Natural Science and Engineering Research Council of Canada (NSERC), the Canada Research Chair Program (CRC), the Canada Foundation for Innovation (CFI), the University of Western Ontario (UWO), and the National Natural Science Fund of China (No. 51602303). X.L., J.L., W.L., and X.L. acknowledge the receipt of support from the CLS Postdoctoral Student Travel Support Program.

DOI: 10.1021/acs.chemmater.8b04987
Chem. Mater. 2019, 31, 2002−2009

REFERENCES

(1) Evers, S.; Nazar, L. F. New approaches for high energy density lithium−sulfur battery cathodes. *Acc. Chem. Res.* **2013**, *46*, 1135−1143.

(2) Ji, X.; Evers, S.; Black, R.; Nazar, L. F. Stabilizing lithium−sulphur cathodes using polysulphide reservoirs. *Nat. Commun.* **2011**, *2*, No. 325.

(3) Chen, C.-Y.; Peng, H.-J.; Hou, T.-Z.; Zhai, P.-Y.; Li, B.-Q.; Tang, C.; Zhu, W.; Huang, J.-Q.; Zhang, Q. A Quinonoid-Imine-Enriched Nanostructured Polymer Mediator for Lithium−Sulfur Batteries. *Adv. Mater.* **2017**, *29*, No. 1606802.

(4) Yang, X.; Li, X.; Adair, K.; Zhang, H.; Sun, X. Structural Design of Lithium−Sulfur Batteries: From Fundamental Research to Practical Application. *Electrochem. Energy Rev.* **2018**, *1*, 239−293.

(5) Gao, J.; Lowe, M. A.; Kiya, Y.; Abruña, H. D. Effects of liquid electrolytes on the charge−discharge performance of rechargeable lithium/sulfur batteries: electrochemical and in-situ X-ray absorption spectroscopic studies. *J. Phys. Chem. C* **2011**, *115*, 25132−25137.

(6) Barchasz, C.; Leprêtre, J.-C.; Patoux, S.; Alloin, F. Electrochemical properties of ether-based electrolytes for lithium/sulfur rechargeable batteries. *Electrochim. Acta* **2013**, *89*, 737−743.

(7) Gu, S.; Sun, C.; Xu, D.; Lu, Y.; Jin, J.; Wen, Z. Recent Progress in Liquid Electrolyte-Based Li−S Batteries: Shuttle Problem and Solutions. *Electrochem. Energy Rev.* **2018**, *1*, 599−624.

(8) Li, Z.; Zhang, J.; Lu, Y.; Lou, X. W. D. A pyrolyzed polyacrylonitrile/selenium disulfide composite cathode with remarkable lithium and sodium storage performances. *Sci. Adv.* **2018**, *4*, No. eaat1687.

(9) Yin, L.; Wang, J.; Lin, F.; Yang, J.; Nuli, Y. Polyacrylonitrile/graphene composite as a precursor to a sulfur-based cathode material for high-rate rechargeable Li−S batteries. *Energy Environ. Sci.* **2012**, *5*, 6966−6972.

(10) Xin, S.; Gu, L.; Zhao, N.-H.; Yin, Y.-X.; Zhou, L.-J.; Guo, Y.-G.; Wan, L.-J. Smaller sulfur molecules promise better lithium−sulfur batteries. *J. Am. Chem. Soc.* **2012**, *134*, 18510−18513.

(11) Li, X.; Liang, J.; Zhang, K.; Hou, Z.; Zhang, W.; Zhu, Y.; Qian, Y. Amorphous S-rich S1-xSex/C ($x \leq 0.1$) composites promise better lithium−sulfur batteries in a carbonate-based electrolyte. *Energy Environ. Sci.* **2015**, *8*, 3181−3186.

(12) Xu, G.-L.; Sun, H.; Luo, C.; Estevez, L.; Zhuang, M.; Gao, H.; Amine, R.; Wang, H.; Zhang, X.; Sun, C. J. Solid-State Lithium/Selenium−Sulfur Chemistry Enabled via a Robust Solid-Electrolyte Interphase. *Adv. Energy Mater.* **2018**, No. 1802235.

(13) Li, X.; Banis, M.; Lushington, A.; Yang, X.; Sun, Q.; Zhao, Y.; Liu, C.; Li, Q.; Wang, B.; Xiao, W.; et al. A high-energy sulfur cathode in carbonate electrolyte by eliminating polysulfides via solid-phase lithium-sulfur transformation. *Nat. Commun.* **2018**, *9*, No. 4509.

(14) Sakuda, A.; Taguchi, N.; Takeuchi, T.; Kobayashi, H.; Sakaebe, H.; Tatsumi, K.; Ogumi, Z. Amorphous niobium sulfides as novel positive-electrode materials. *ECS Electrochem. Lett.* **2014**, *3*, A79−A81.

(15) Truong, Q. D.; Kempaiah Devaraju, M.; Nguyen, D. N.; Gambe, Y.; Nayuki, K.; Sasaki, Y.; Tran, P. D.; Honma, I. Disulfide-bridged (Mo3S11) cluster polymer: Molecular dynamics and application as electrode material for a rechargeable magnesium battery. *Nano Lett.* **2016**, *16*, 5829−5835.

(16) Ye, H.; Ma, L.; Zhou, Y.; Wang, L.; Han, N.; Zhao, F.; Deng, J.; Wu, T.; Li, Y.; Lu, J. Amorphous MoS3 as the sulfur-equivalent cathode material for room-temperature Li−S and Na−S batteries. *Proc. Natl. Acad. Sci. U.S.A.* **2017**, *114*, 13091−13096.

(17) Sakuda, A.; Ohara, K.; Fukuda, K.; Nakanishi, K.; Kawaguchi, T.; Arai, H.; Uchimoto, Y.; Ohta, T.; Matsubara, E.; Ogumi, Z.; et al. Amorphous metal polysulfides: electrode materials with unique insertion/extraction reactions. *J. Am. Chem. Soc.* **2017**, *139*, 8796−8799.

(18) Hu, Z.; Zhang, K.; Zhu, Z.; Tao, Z.; Chen, J. FeS2 microspheres with an ether-based electrolyte for high-performance rechargeable lithium batteries. *J. Mater. Chem. A* **2015**, *3*, 12898−12904.

(19) Zabel, J.; Nair, R. R.; Ott, A.; Georgiou, T.; Geim, A. K.; Novoselov, K. S.; Casiraghi, C. Raman spectroscopy of graphene and bilayer under biaxial strain: bubbles and balloons. *Nano Lett.* **2012**, *12*, 617−621.

(20) Duan, B.; Wang, W.; Wang, A.; Yu, Z.; Zhao, H.; Yang, Y. A new lithium secondary battery system: the sulfur/lithium-ion battery. *J. Mater. Chem. A* **2014**, *2*, 308−314.

(21) Wei, S.; Ma, L.; Hendrickson, K. E.; Tu, Z.; Archer, L. A. Metal−Sulfur Battery Cathodes Based on PAN−Sulfur Composites. *J. Am. Chem. Soc.* **2015**, *137*, 12143−12152.

(22) Tamor, M.; Vassell, W. Raman "fingerprinting"of amorphous carbon films. *J. Appl. Phys.* **1994**, *76*, 3823−3830.

(23) Doan-Nguyen, V. V.; Subrahmanyam, K. S.; Butala, M. M.; Gerbec, J. A.; Islam, S. M.; Kanipe, K. N.; Wilson, C. E.; Balasubramanian, M.; Wiaderek, K. M.; Borkiewicz, O. J.; et al. Molybdenum polysulfide chalcogels as high-capacity, anion-redox-driven electrode materials for Li-ion batteries. *Chem. Mater.* **2016**, *28*, 8357−8365.

(24) Tran, P. D.; Tran, T. V.; Orio, M.; Torelli, S.; Truong, Q. D.; Nayuki, K.; Sasaki, Y.; Chiam, S. Y.; Yi, R.; Honma, I.; et al. Coordination polymer structure and revisited hydrogen evolution catalytic mechanism for amorphous molybdenum sulfide. *Nat. Mater.* **2016**, *15*, 640−646.

(25) Paraknowitsch, J. P.; Thomas, A.; Schmidt, J. Microporous sulfur-doped carbon from thienyl-based polymer network precursors. *Chem. Commun.* **2011**, *47*, 8283−8285.

(26) Newville, M. Fundamentals of XAFS. *Rev. Mineral. Geochem.* **2014**, *78*, 33−74.

(27) Tryk, D. A.; Kim, S.; Hu, Y.; Xing, W.; Scherson, D. A.; Antonio, M. R.; Leger, V. Z.; Blomgren, G. E. Electrochemical Insertion of Lithium into Pyrite from Nonaqueous Electrolytes at Room Temperature: An in situ Fe K-Edge X-ray Absorption Fine Structure Study. *J. Phys. Chem. C* **1995**, *99*, 3732−3735.

(28) Bowden, W. L.; Barnette, L. H.; Demuth, D. L. Transition metal polysulfides as battery cathodes. *J. Electrochem. Soc.* **1988**, *135*, 1−6.

(29) Shimoda, K.; Murakami, M.; Takeuchi, T.; Matsunaga, T.; Ukyo, Y.; Sakaebe, H.; Kobayashi, H.; Matsubara, E. Structural and dynamic behavior of lithium iron polysulfide Li8FeS5 during charge−discharge cycling. *J. Power Sources* **2018**, *398*, 67−74.

(30) Ye, H.; Wang, L.; Deng, S.; Zeng, X.; Nie, K.; Duchesne, P. N.; Wang, B.; Liu, S.; Zhou, J.; Zhao, F.; et al. Amorphous MoS3 Infiltrated with Carbon Nanotubes as an Advanced Anode Material of Sodium-Ion Batteries with Large Gravimetric, Areal, and Volumetric Capacities. *Adv. Energy Mater.* **2017**, *7*, No. 1601602.

(31) Markevich, E.; Salitra, G.; Talyosef, Y.; Chesneau, F.; Aurbach, D. On the Mechanism of Quasi-Solid-State Lithiation of Sulfur Encapsulated in Microporous Carbons: Is the Existence of Small Sulfur Molecules Necessary? *J. Electrochem. Soc.* **2017**, *164*, A6244−A6253.

(32) Helen, M.; Reddy, M. A.; Diemant, T.; Golla-Schindler, U.; Behm, R. J.; Kaiser, U.; Fichtner, M. Single step transformation of sulphur to Li2S2/Li2S in Li-S batteries. *Sci. Rep.* **2015**, *5*, No. 12146.

(33) Chastain, J.; King, R. C.; Moulder, J. *Handbook of X-ray Photoelectron Spectroscopy: A Reference Book of Standard Spectra for Identification and Interpretation of XPS Data*; Physical Electronics Division, Perkin-Elmer Corporation Eden Prairie: Minnesota, 1992.

(34) Wang, L.; Wang, Y.; Xia, Y. A high performance lithium-ion sulfur battery based on a Li 2 S cathode using a dual-phase electrolyte. *Energy Environ. Sci.* **2015**, *8*, 1551−1558.

DOI: 10.1021/acs.chemmater.8b04987
Chem. Mater. 2019, 31, 2002−2009